# Two-Dimensional Photogalvanic Spin-Battery

Yiqun Xie,[1,2] Mingyan Chen,[1,2,3] Zewen Wu,[2,4] Yibin Hu,[5] Yin Wang,[2,6,*] Jian Wang,[2] and Hong Guo[2,7]

[1] *Department of Physics, Shanghai Normal University, 100 Guilin Road, Shanghai 200232, China*
[2] *Department of Physics and the Center of Theoretical and Computational Physics, The University of Hong Kong, Pokfulam Road, Hong Kong SAR, China*
[3] *Hongzhiwei Technology (Shanghai) Co., Ltd., 1888 Xinjinqiao Road, Shanghai 201206, China*
[4] *Department of Physics, Beijing Institute of Technology, Beijing 100081, China*
[5] *National Laboratory for Infrared Physics, Shanghai Institute of Technical Physics, Chinese Academy of Sciences, Shanghai 200083, China*
[6] *Department of Physics and International Centre for Quantum and Molecular Structures, Shanghai University, 99 Shangda Road, Shanghai 200444, China*
[7] *Center for the Physics of Materials and Department of Physics, McGill University, Montreal, Quebec H3A 2T8, Canada*

(Received 4 March 2018; revised manuscript received 21 July 2018; published 5 September 2018)

Pure spin current is of central importance in spintronics. Here, we propose a two-dimensional (2D) spin-battery system that delivers pure spin current without an accompanying charge current to the outside world at zero bias. The principle of the spin battery is rooted in the photogalvanic effect (PGE) and the system has good operational stability against structural perturbation, photon energy, and other material characteristics. The principle of the device is numerically implemented in the 2D material phosphorene as an example, and first-principles calculations give excellent qualitative agreement with the physics of the PGE. The 2D spin battery is interesting as it is both a device that generates pure spin currents and also an energy source that harvests photons. Given the versatile operational space, the spin battery should be experimentally feasible.

DOI: 10.1103/PhysRevApplied.10.034005

## I. INTRODUCTION

Two-dimensional (2D) materials are important for applications in logic and photonic devices, solar cells, transparent substrates, and, most interestingly, wearable electronics [1]. The thin body in 2D makes them the natural choice for the production of flexible structures. The spin physics of 2D materials is central for flexible spintronics, which requires less power to operate [2–5]. In flexible applications, self-powered systems—by harvesting photons, for example—are extremely helpful [2]. It is the purpose of this work to propose and investigate a 2D photogalvanic spin battery that generates pure spin current without an accompanying charge current, for 2D spintronics.

The photogalvanic effect (PGE) is an optoelectronic phenomenon that occurs in materials without a spatial inversion symmetry [6]. A *direct* charge current is generated to flow by the PGE with neither an external bias voltage nor an internal electric field like that inside the $p$-$n$ junction of photocells. The PGE is purely a *nonlinear* and *symmetry-induced* optical response of materials to light, $j \sim \alpha \boldsymbol{E}\boldsymbol{E}^*$, where $j$ is the PGE photocurrent, $\boldsymbol{E}$ is the electric field of the light, and $\alpha$ the PGE coefficient. Because reversing the direction of $\boldsymbol{E}$ will reverse the flow of current, from $j$ to $-j$, $j$ must vanish unless $\alpha$ also changes its sign, which can only occur when the material has no spatial inversion symmetry [6]. A device operating on the PGE can deliver a dc electric current to the outside world in closed circuit, i.e., like a battery. Recent experimental demonstrations of the PGE include the use of silicon nanowires [7] and Si metal-oxide-semiconductor field-effect transistors (MOSFETs) [8,9], where the inversion symmetry was broken by the geometry of the device.

The PGE has been exploited to generate spin-polarized charge currents [10–14], typically in materials having a strong spin-orbit coupling (SOC) including transition-metal dichalcogenides [15,16] and topological insulators [17–19]. These materials lift spin degeneracy by SOC so that spin-up and -down electrons are photoexcited by left- and right-circularly polarized light governed by the optical selection rule, to produce a spin-polarized photocurrent $I_{\rm ph} = I_\uparrow + I_\downarrow$, where $I_\uparrow, I_\downarrow$ are contributions from the

*yinwang@shu.edu.cn

 

spin-up and -down channels. Clearly, accompanying the charge current $I_{\rm ph}$, there is also a spin current $I_s = I_\uparrow - I_\downarrow$, which is nonzero if $I_\uparrow \neq I_\downarrow$. A most interesting situation is when $I_\uparrow = -I_\downarrow$, i.e., the spin-up and -down channels flow in exactly opposite directions. When this happens, a *pure* spin current $I_s$ flows without an accompanying charge current $I_{\rm ph}$. Pure spin current is prominent in spintronics [3], spin caloritronics [20,21], the spin Hall effect [22,23], spin pumping [24–26], and the spin Seebeck effect [27–31], where SOC plays the key role in lifting the spin degeneracy and/or inducing a transverse anomalous velocity.

Can the PGE provide a physical principle of a device that generates pure spin current without the aid of SOC? Indeed, in a broad category of materials consisting light elements such as carbon, SOC is negligibly weak. Since there is no SOC, we consider such a device design (hereafter named the spin battery) in the form of a thin semiconductor (S) barrier sandwiched between two ferromagnetic metal (FM) contacts. The FM-S-FM structure is widely used in tunnel junctions where both spin-up and -down electrons flow from one FM through the semiconductor to the other FM, i.e., a flow of spin-polarized charge current accompanied by a spin current [32–35]. By means of the PGE, however, we show that the spin battery can generate a pure $I_s$ that flows out of the system without any charge current and, in open circuit, a spin-resolved chemical potential difference is established on the two sides of the device due to the action of the PGE.

## II. PHYSICS OF THE PGE SPIN BATTERY

The proposed PGE spin battery is in the form of a FM-S-FM structure in open circuit, and in closed circuit it is part of a two-probe structure, (FM-electrode)+(FM-S-FM)+(FM-electrode), shown in Fig. 1. We assume that there is no spatial inversion symmetry and, for simplicity of the discussion, let us consider the central region to be mirror symmetric across the middle (the $C_s$ point group). The semiconductor has an appropriate band gap for photon adsorption. Without loss of generality, we implement the idea in two-dimensional (monolayer) black phosphorous, called phosphorene as the semiconductor, sandwiched by nickel FM contacts. Phosphorene has attractive electronic and optical properties, including significant carrier mobility [36], a direct band gap [37,38], a broadband photoresponse [39–42], and spin transmission [43,44]. We emphasize that the physics of the PGE spin battery is general and that the choice of semiconductor is not restricted to phosphorene.

Before discussing the principle of the spin battery, let us outline the PGE from the point of view of photoexcitation, using Fig. 1(b), which describes spin-degenerate case by replacing the FM metal with nonmagnetic metal such as Cu or Au. By absorbing photons, electrons are excited from the valence bands (VBs) to the conduction bands (CBs),

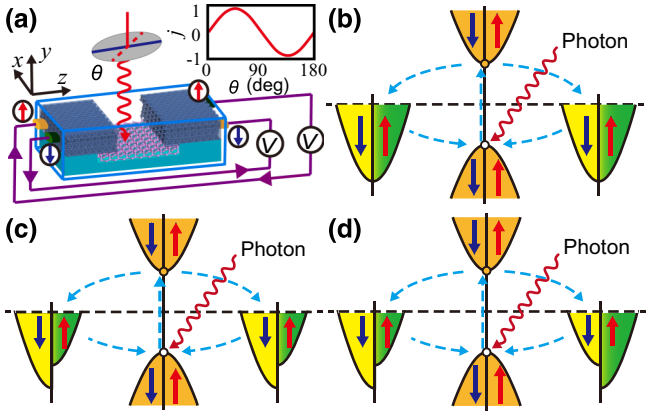


FIG. 1. (a) A schematic diagram of the spin battery, which is a FM-semiconductor-FM structure under illumination by polarized light, as shown in the blue cuboid. The spin-down and -up electrons come out from the system, flow through the external circuit, and, finally, go back to the spin battery via the orange electrode. (b) The band diagram of spin-degenerate case. (c) The band diagram for a parallel configuration (PC) of two FMs in the system. (d) The band diagram for an antiparallel configuration (APC) of the two FMs: this is the spin-battery device. The blue dashed lines with arrows indicate electron transitions.

and they flow out of the semiconductor to the left or right. At the same time, the holes left in the VBs are filled by electrons coming from the two metals. These processes are indicated in Fig. 1(b) by the blue dashed lines. When incident light is polarized in parallel (polarization angle $\theta = 90°$) or perpendicular ($\theta = 0°,\ 180°$) to the mirror reflection plane, $C_s$ symmetry is maintained and due to this mirror symmetry, excited electrons have exactly the same probability of flowing to the left or to the right, resulting in a zero photocurrent. For other polarization angles $\theta$, the coupling of polarized photons and electrons in the semiconductor breaks the mirror symmetry; hence photoexcited electrons have different probabilities of flowing to the left or to the right, resulting in a net photogalvanic current $I_{\rm ph}$ at zero bias. This PGE current has a distinct dependence on the polarization angle $\theta$, e.g., it varies as $\sin(2\theta)$ for the case of $C_s$ symmetry.

The physical origin of the photocurrent generated by the PGE can be understood from the standard phenomenological theory [6]. For a material with $C_s$ symmetry, the photocurrent under normal incidence of linearly polarized light is described by

$$j_z = E_0^2 \chi_{zzx} \sin(2\theta), \quad j_x = E_0^2[\chi_+ + \chi_- \cos(2\theta)]. \quad (1)$$

Here, $j_z$ and $j_x$ are the photocurrents along the directions normal and parallel to the mirror reflection plane, respectively. For circularly polarized light,

$$j_z = E_0^2 \gamma_{zy} \sin(2\phi), \quad j_x = E_0^2[\chi_+ + \chi_- \cos(2\phi)]. \quad (2)$$

In Eqs. (1) and (2), $E_0^2$ is the electric-field amplitude of the light and $\chi_{zzx}$, $\chi_+$, $\chi_-$, and $\gamma_{zy}$ are tensors that depend on the photon frequency $\omega$. Therefore, the PGE is essentially a second-order response to the electric field. In this scenario, the light illumination contributes to the response coefficients $\chi_{zzx}$, $\chi_+$, $\chi_-$, and $\gamma_{zy}$, and thus generates a PGE photocurrent. Therefore, the behavior of the photocurrent either takes a sine or a cosine dependence on the light polarization, determined by both the light and the symmetry of the system.

Having understood the ordinary PGE, we now discuss cases with spins. If the magnetic moments of the two FMs in the spin battery are in a parallel configuration (PC) as shown in Fig. 1(c), photoexcited electrons—regardless of their spin—act in just the same way as in the nonmagnetic case, because the two spin channels are not coupled (no SOC). Consequently, a spin-polarized charge current $I_{\rm ph}$ is generated by the PGE when $\theta$ is not $0^\circ$, $90^\circ$, or $180^\circ$.

Finally, if the magnetic moments of the FMs are in an antiparallel configuration (APC) as shown in Fig. 1(d), the $C_s$ mirror reflection symmetry of the device for *individual* spin channel is broken by the majority and/or minority density of states in the FMs. Then, both spin-up and -down PGE currents $I_\uparrow$ and $I_\downarrow$ are generated for *all* angles $\theta$, including at $\theta = 0^\circ$, $90^\circ$, and $180^\circ$. Note that even though the spin distribution is different in APC as compared to PC, the *charge distribution* is the same in PC and APC (and also in the nonmagnetic case). Therefore the total *charge current* $I_{\rm ph} = I_\uparrow + I_\downarrow$ must behave in the same way as that in PC and/or in the nonmagnetic case, namely $I_{\rm ph}$ must vanish at $\theta = 0^\circ$, $90^\circ$ and $180^\circ$. We therefore arrive at a most interesting conclusion for APC: namely, since $I_\uparrow$ and $I_\downarrow$ are nonzero at $\theta = 0^\circ$, $90^\circ$, and $180^\circ$ due to the PGE but $I_{\rm ph}$ vanishes at these angles, $I_\uparrow$ and $I_\downarrow$ must be equal in magnitude but must flow in exactly opposite directions. In other words, for a device without inversion symmetry but that is mirror symmetric, a nonzero spin current $I_s$ without an accompanying charge current $I_{\rm ph}$ can be generated by the PGE in APC. This device behaves as a spin battery because in open circuit, a spin-resolved chemical potential difference is established on the two sides of the device due to the action of the PGE. The device in Fig. 1(d) is the pure spin battery, which will be the focus of the rest of the paper.

Having qualitatively understood the pure spin battery, we now implement the idea using 2D phosphorene as the semiconductor. The phosphorene has a puckered structure with four P atoms in a primitive cell, as shown in Fig. 2(a). It has a spatial inversion symmetry that belongs to the $D_{2h}$ point group, with the inversion center located between atoms 2 and 3, as indicated in Fig. 2(a). This means that the symmetry is invariant when interchanging atoms 1, 2, and 6 with atoms 5, 3, and 4, respectively. To have the PGE, it is essential to break this intrinsic inversion symmetry. This is actually not difficult because the local Schottky electric field formed at the metal-phosphorene contacts breaks the inversion symmetry, as shown experimentally (albeit in a different material) [7].

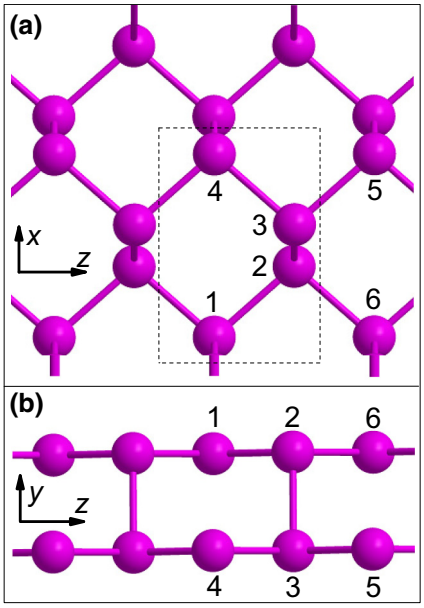


FIG. 2. The (a) top and (b) side views of the 2D phosphorene. The dashed lines in (a) indicate the rectangle primitive cell of the phosphorene, which has four atoms.

## III. MODEL AND METHODS

In light of the physics of the proposed spin battery, we construct a FM-S-FM structure, the energy diagram of which is shown in Figs. 1(c) and 1(d), where the FM is nickel (Ni) and the semiconductor is phosphorene, as shown in Fig. 3(a). Phosphorene has a $C_s$ symmetry in which the zigzag direction is perpendicular to the mirror reflection plane. Again, the formation of a Ni-phosphorene interface leads to a Schottky potential that breaks the inversion symmetry of phosphorene [7]. For instance, the electrostatic potential at atom 2 does not equal that at atom 3, owing to the broken inversion symmetry. Note that the central region of the spin battery is a Ni-phosphorene-Ni composite system.

The device model consists of three parts, including the left- and right-hand nickel electrodes and the center region, as shown in Fig. 3(a). The electrodes are modeled by a five-layer Ni(111) slab consisting of $2 \times 3$ atoms in each layer, and the two electrodes extend to $z = \pm\infty$, respectively. The left- and right-hand electrodes are the mirror images of each other. In the center region, the phosphorene bridges and partially overlaps the two Ni(111) electrodes, with a vertical Ni-P distance of 2.0 Å, determined by the VASP calculation [45]. The whole system periodically extends in the $x$ direction with a periodicity of 4.316 Å. The calculated lattice constants of the phosphorene are $a = 3.32$ Å and $b = 4.58$ Å, which is homogeneously strained by about

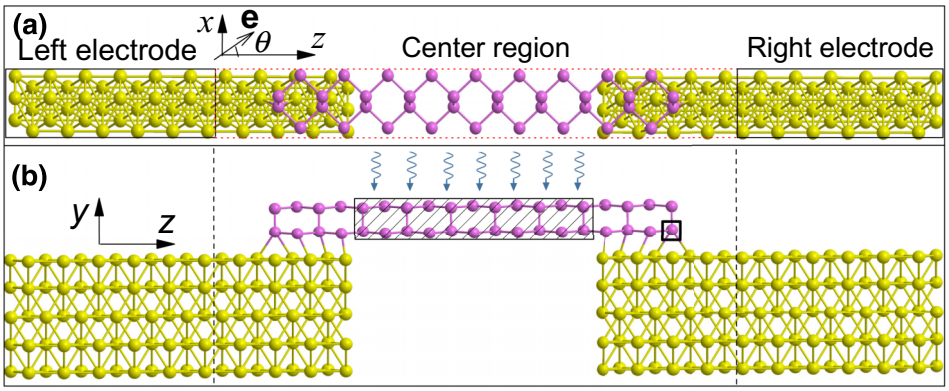


FIG. 3. The (a) top view and (b) side view of the structure of the two-probe device for calculating the photocurrent of the phosphorene phototransistor. The yellow spheres denote Ni atoms and the others are P atoms. The light (arrows) is shed in the $y$ direction, perpendicularly to the phosphorene in the $x$-$z$ plane. $\theta$ is the polarization angle for linearly polarized light and $\mathbf{e}$ is the polarization vector. The shaded area in (b) denotes the P atoms illuminated by the light, and the P atom in the rectangular box will be replaced by a As atom (see the main text).

$-5.7\%$ in order to match the Ni lattice in the $x$ direction. The band gap of the phosphorene is 1.03 eV, calculated using the local density approximation.

The pristine phosphorene has a spatial inversion symmetry and belongs to the $D_{2h}$ point group, with a mirror reflection plane (the $x$-$y$ plane) perpendicular to the zigzag ($z$) direction. However, the contact with the electrodes breaks the $D_{2h}$ symmetry of the pristine phosphorene, as can easily be seen from the side view of the center region shown in Fig. 3(b), even though the mirror reflection plane (the $x$-$y$ plane) still remains, as can be observed from Fig. 3(a). Thus the phototransistor possesses $C_s$ symmetry, owing to which we can obtain a spin-polarized photocurrent generated by the PGE.

We have developed a theoretical approach to calculating the photocurrent generated by the PGE based on density-functional theory within the nonequilibrium Green's function (NEGF-DFT) formalism [46] and implemented it in the first-principles quantum-transport package NANODCAL [47]. Specifically, for linearly polarized light, the photocurrent injected into the lead $L$ can be written as follows [46]:

$$J_L^{(\mathrm{ph})} = \frac{ie}{h}\int\Big(\cos^2\theta\,\mathrm{Tr}\{\Gamma_L[G_1^{<(\mathrm{ph})} + f_L(G_1^{>(\mathrm{ph})} - G_1^{<(\mathrm{ph})})]\} + \sin^2\theta\,\mathrm{Tr}\{\Gamma_L[G_2^{<(\mathrm{ph})} + f_L(G_2^{>(\mathrm{ph})} - G_2^{<(\mathrm{ph})})]\} + \frac{\sin(2\theta)}{2}\mathrm{Tr}\{\Gamma_L[G_3^{<(\mathrm{ph})} + f_L(G_3^{>(\mathrm{ph})} - G_3^{<(\mathrm{ph})})]\}\Big)dE, \tag{3}$$

where

$$G_1^{>/<(\mathrm{ph})} = \sum_{\alpha,\beta=x,y,z} C_0 N G_0^r e_{1\alpha} p_\alpha^\dagger G_0^{>/<} e_{1\beta} p_\beta G_0^a,$$

$$G_2^{>/<(\mathrm{ph})} = \sum_{\alpha,\beta=x,y,z} C_0 N G_0^r e_{2\alpha} p_\alpha^\dagger G_0^{>/<} e_{2\beta} p_\beta G_0^a,$$

$$G_3^{>/<(\mathrm{ph})} = \sum_{\alpha,\beta=x,y,z} C_0 N (G_0^r e_{1\alpha} p_\alpha^\dagger G_0^{>/<} e_{2\beta} p_\beta G_0^a + G_0^r e_{2\alpha} p_\alpha^\dagger G_0^{>/<} e_{1\beta} p_\beta G_0^a). \tag{4}$$

For circularly polarized light, we obtain

$$J_L^{(\mathrm{ph})} = \frac{ie}{h}\int\Big(\cos^2\phi\,\mathrm{Tr}\{\Gamma_L[G_1^{<(\mathrm{ph})} + f_L(G_1^{>(\mathrm{ph})} - G_1^{<(\mathrm{ph})})]\} + \sin^2\phi\,\mathrm{Tr}\{\Gamma_L[G_2^{<(\mathrm{ph})} + f_L(G_2^{>(\mathrm{ph})} - G_2^{<(\mathrm{ph})})]\} + \frac{\sin(2\phi)}{2}\mathrm{Tr}\{\Gamma_L[G_3^{<(\mathrm{ph})} + f_L(G_3^{>(\mathrm{ph})} - G_3^{<(\mathrm{ph})})]\}\Big)dE, \tag{5}$$

where $G_{1,2}^{>/<(\mathrm{ph})}$ is same as in the linearly polarized case and

$$G_3^{>/<(\mathrm{ph})} = \pm i\sum_{\alpha,\beta=x,y,z} C_0 N (G_0^r e_{1\alpha} p_\alpha^\dagger G_0^{>/<} e_{2\beta} p_\beta G_0^a - G_0^r e_{2\alpha} p_\alpha^\dagger G_0^{>/<} e_{1\beta} p_\beta G_0^a). \tag{6}$$

In Eqs. (4) and (6), $C_0 = (e/m_0)^2(\hbar\sqrt{\mu_r\epsilon_r}/2N\omega\epsilon c)I_\omega$, where $m_0$ is the bare electron mass; $I_\omega$ is the photon flux, defined as the number of photons per unit time per unit area; $\omega$ is the frequency and $c$ is the speed of light; $\mu_r$ is the relative magnetic susceptibility; $\epsilon_r$ is the relative dielectric constant; $\epsilon$ is the dielectric constant; and $N$ is the number of photons. In the above expressions, $G_0^{r/a}$ are the retarded and advanced Green's functions without photons, respectively, and $G_0^{>/<}$ are the greater and lesser Green's function without photons, respectively. $p_{x,y,z}$ is the Cartesian component of the electron momentum, and $e_{1/2x,y,z}$ is the Cartesian component of the unit vector $\mathbf{e}_{1/2}$, which characterizes the polarization of the light. For elliptically polarized light,

the polarization vector $\mathbf{e} = \cos\phi\mathbf{e}_1 \pm i\sin\phi\mathbf{e}_2$, where "±" denotes the right- and/or left-handed elliptical light, and $\phi$ determines its helicity. In particular, $\phi = \pm 45^o$ corresponds to circularly polarized light. For linearly polarized light, $\mathbf{e} = \cos\theta\mathbf{e}_1 + \sin\theta\mathbf{e}_2$, where $\theta$ is the angle formed by the polarization direction with respect to the vector $\mathbf{e}_1$. We calculate a normalized photocurrent, i.e., the photoresponse function written as $R = J_L^{(\mathrm{ph})}/eI_\omega$, which still has a dimension of area, i.e., $a_0^2$ per phonon, where $a_0$ is the Bohr radius. We note that for laser power of 0.1–105 W/cm$^2$ with an illumination area of 1 $\mu$m$^2$, the calculated photocurrent ranges from 1 pA to 1 $\mu$A, which can be measured experimentally [41,48].

We calculate the PGE current along the zigzag ($z$) phosphorene direction under linearly or circularly polarized light vertically incident to the phosphorene ($y$ direction), indicated by the wiggly arrows in Fig. 3(b). The light is polarized in the $x$-$z$ plane, and for linearly polarized light the polarization vector $\mathbf{e}$ forms an angle $\theta$ with respect to the zigzag direction. A wide range of photon energies from 1.2 to 2.0 eV are investigated. SOC is not considered to reduce computational cost: we verify that including SOC does not qualitatively change any of the results. In the NEGF-DFT numerical calculations, the double-zeta polarized (DZP) atomic orbital basis is used to expand all the physical quantities; the exchange and correlation are treated at the level of local density approximation; and atomic cores are defined by the standard norm, conserving nonlocal pseudopotentials. In the self-consistent calculations and the photocurrent transport calculations of the two-probe device structures (Fig. 3), $16 \times 1 \times 1$ $k$-points are used. These calculation details are verified to obtain converging results. Unless otherwise specified, collinear spin is used for the NEGF-DFT calculations in which spin polarizations at different places are all along the same direction, in either PC or APC.

## IV. RESULTS AND DISCUSSION

### A. The PGE spin battery

We first consider the case of PC [see Fig. 1(c)], for which the calculated PGE photocurrent versus the polarization angle $\theta$ for linearly polarized light is presented in Fig. 4(a). The PGE photocurrent is spin polarized and both $I_\uparrow$ and $I_\downarrow$ vary as $\sin(2\theta)$ and have opposite sign (i.e., the opposite flow direction). Specifically, $I_\uparrow$ (red square) and $I_\downarrow$ (blue sphere) are well fitted as $I_\uparrow \approx -0.041 \times \sin(2\theta)$ (red line) and $I_\downarrow \approx 0.006 \times \sin(2\theta)$ (blue line), respectively. Consequently, the total PGE charge current, $I_{\mathrm{ph}} = I_\uparrow + I_\downarrow$ (dark triangles), also has a sinusoidal shape (black line), which is a characteristic feature of the linear photogalvanic effect (LPGE) [6,11]. For circularly polarized light, Fig. 4(b) shows that the $I_\uparrow$ and $I_\downarrow$ have the same sign, and both vary in terms of $\sin(2\phi)$, where $\phi$ is the helicity of circularly polarized light. The photocurrents are also well fitted with sine functions (lines), as shown in Fig. 4(b). The sine dependence of the photocurrent on the helicity of circularly polarized light is the well-known circular PGE (CPGE) [11–14]. These numerical results are perfectly consistent with the qualitative discussion above: for instance, at $\theta = 0^\circ$, $90^\circ$, and $180^\circ$, $I_\uparrow$, $I_\downarrow$ and $I_{\mathrm{ph}}$ all vanish, as argued above by the PC model of Fig. 1(c).

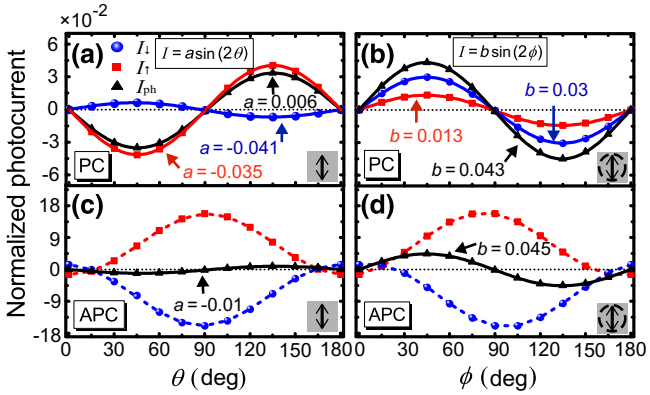


FIG. 4. The spin-up ($I_\uparrow$), spin-down ($I_\downarrow$), and total photocurrent ($I_{\mathrm{ph}}$) under linearly and circularly polarized light (a),(b) in PC and (c),(d) in APC. The symbols denote the calculated results and the solid lines denote the fitted ones.

The variation of the PGE current in terms of $\sin(2\theta)$ or $\sin(2\phi)$ under linearly or circularly polarized light is the typical behavior of the PGE determined by the $C_s$ symmetry. According to the phenomenological theory of the PGE [6], whether the photocurrent is a sine or a cosine depends on the symmetry. For systems with $C_s$ symmetry, the photocurrent generated in the direction perpendicular to the mirror reflection plane is a sine, which is in perfect agreement with our first-principles results presented here. Note that the phenomenological theory has been widely adopted to explain experimental observations of the LPGE and the CPGE; for instance, for $p$-GaAs-(Al,Ga)As quantum-well systems having $C_s$ symmetry [11].

As argued in the qualitative discussion above, the pure spin battery is established by the device in APC [see Fig. 1(d)], for which the calculated photocurrents due to the LPGE and CPGE are shown in Figs. 4(c) and 4(d), respectively. The total photocurrents (dark triangles) are exactly in the shape of $\sin(2\theta)$ for the LPGE or $\sin(2\phi)$ for the CPGE, and are well fitted by the sine functions (dark lines). In contrast, for individual spin channels, $I_\uparrow$ and $I_\downarrow$ have opposite sign and appear more like a cosine function. As a result, at $\theta, \phi = 0^\circ$, $90^\circ$, and $180^\circ$, the calculated total PGE charge current $I_{\mathrm{ph}}$ is essentially zero, while the spin current $I_s = I_\uparrow - I_\downarrow$ is nonzero. Namely, the spin battery generates a pure spin current without an accompanying charge current at these polarization angles. The calculated data are perfectly consistent with the qualitative discussion above.

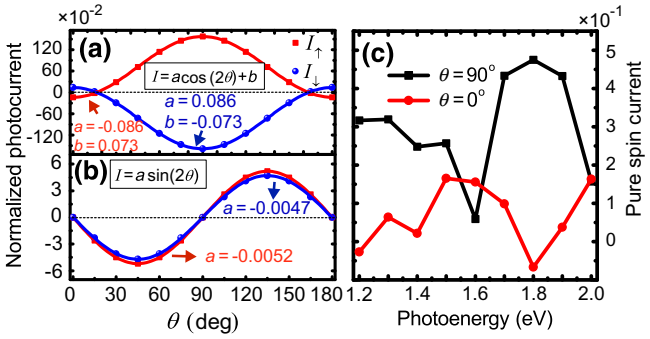


FIG. 5. (a),(b) Two components of the photocurrent, proportional to $\cos(2\theta)$ and $\sin(2\theta)$, respectively, under illumination by linearly polarized light for APC (the spin battery). The symbols are calculated data and the solid lines are fitted to the data. (c) Operational points of an ideal spin battery for both linearly and circularly polarized light. The data points give values of the photon energy and polarization angle $\theta$, where pure spin currents without an accompanying charge current are generated.

To further understand the origin of the pure spin current generated by the spin battery, we now analyze the photocurrent which, if generated by linearly polarized light, has three components, proportional to $\sin^2(\theta)$, $\cos^2(\theta)$, and $\sin(2\theta)$, respectively [Eq. (1)]. The first two components can be expressed in terms of $\cos(2\theta)$. In APC (the spin battery), the charge distribution in the device retains $C_s$ symmetry, since the antiparallel spin configuration does not influence the charge distribution, as mentioned above. Therefore, $I_{\rm ph}$ should be proportional to $\sin(2\theta)$. However, the spin distribution of the system is no longer mirror symmetric in APC; therefore the two spin-resolved currents $I_\uparrow$, $I_\downarrow$, should neither be a perfect sine function nor a perfect cosine function. For linearly polarized light, $I_\uparrow$ and $I_\downarrow$ have both $\cos(2\theta)$ and $\sin(2\theta)$ components, although the former has a much larger amplitude, as shown in Figs. 5(a) and 5(b). It is thus concluded that $I_\uparrow$ and $I_\downarrow$ flow in opposite directions with the same magnitude at $\theta = 0°$, $90°$, and $180°$, as the total photocurrent $I_{\rm ph} = I_\uparrow + I_\downarrow$ vanishes due to its sine dependence on $2\theta$. A similar argument holds for circularly polarized light. Therefore, in APC or the spin battery, the PGE generates a pure spin current at polarization angles $\theta, \phi = 0°, 90°$, and $180°$. These results are as expected given the model presented in Fig. 1(d), and are also understandable from the phenomenological point of view [6].

Our calculations show that linearly and circularly polarized light generate the same pure spin current at $\theta = 0°$ and also at $\theta = 90°$, which is also to be expected, as at these angles circularly polarized light has only one polarization vector and hence is equivalent to linearly polarized light. Figure 5(c) plots the calculated operational points of the spin battery in terms of the photon energy in the range of 1.2–2.0 eV and polarization angle $\theta$. Namely, at the calculated data points, the spin battery delivers pure spin currents without an accompanying charge current.

The PGE spin battery is not limited to phosphorene but applicable in general as long as the appropriate symmetry condition is satisfied. For example, if we substitute the newly reported 2D puckered arsenene [49–51] for the phosphorene, we should also be able to generate pure spin current due to a similar structural symmetry. The flow of pure spin current without an accompanying charge current is usually detected via the inverse spin Hall effect [23,52,53]. For the PGE spin battery, the characteristic sinusoidal dependence of the photocurrent is convenient and can serve as evidence for the successful generation of pure spin current; namely, the PGE spin battery not only generates pure spin current but also provides detection by itself. Very interestingly, a recent experiment has reported a persistent photocurrent in phosphorous consisting of a few layers at zero source-drain bias [41]. While the measured data were not interpreted by the physics of the PGE [6], the form of the observed photocurrent versus polarization angle $\theta$ suggests that it was likely due to the PGE. We conclude that a 2D PGE in materials without SOC, such as phosphorene, is quite feasible and that the PGE spin battery is realizable.

### B. The PGE spin battery with disorders and SOC

The symmetry property of the spin-battery structure is so far emphasized in order to interpret the results. In reality, an absolutely perfect symmetry (e.g., $C_s$) is difficult to achieve due to experimental factors such as the existence of impurities and slight differences in the two Ni-phosphorene contacts. Hence the stability against such perturbations should be examined. With regard to the effects of impurity, a recent experiment has shown that phosphorene can be alloyed with As atoms up to 80% As concentration [50]. We thus investigate a system by substituting an As atom for the rightmost P atom in the bottom sublayer of the phosphorene [see Fig. 3(a)]. Concerning asymmetry in the two Ni-phosphorene contacts, we investigate a system by displacing the right Ni contact and the connected Ni(111) substrate in the central region by 0.2 Å along the $x$ direction, corresponding to a mismatch of 4.63% relative to the lattice constant (4.316 Å) of the Ni(111) surface in the $x$ direction. Both of these changes break the $C_s$ symmetry of the original ideal spin battery in Fig. 1(d). The calculated photocurrent becomes that presented in Figs. 6(a) and 6(b) and several observations are in order. First, the PGE photocurrent changes from the perfect $\sin(2\theta)$ of the ideal spin battery to a form $\sin(2\theta + \delta\theta) + C$, where $\delta\theta$ and $C$ are a phase shift and a constant depending on the photon energy, as shown by different curves in Figs. 6(a) and 6(b). Second, compared with the results for the ideal spin battery, the photocurrent is not so much affected by the As impurity, as shown

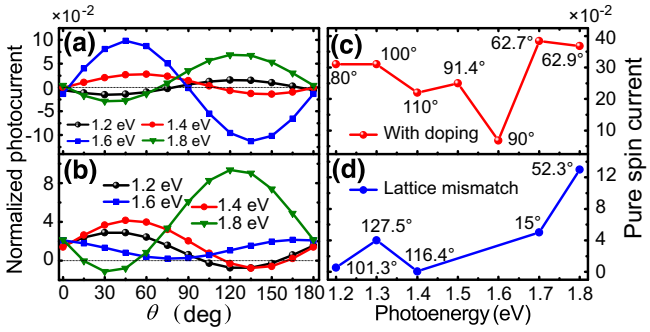


FIG. 6. The photocurrent at different photon energies of linearly polarized light for (a) the doping of the As atoms and (b) the displacement of the right-hand Ni(111) contact in the spin battery. (c) The operational points of the nonideal spin battery doped with As atoms and (d) with contact asymmetry. The data points give values of the photon energy and polarization angle $\theta$, where pure spin currents without an accompanying charge current are generated.

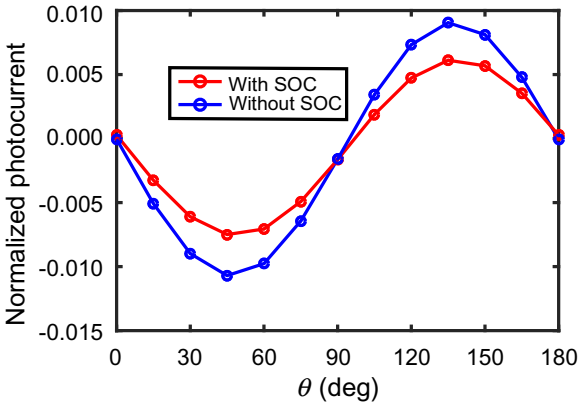


FIG. 7. The total photocurrent versus the polarization angle for the photon energy of 1.2 eV with and without considering spin-orbital coupling.

in Fig. 6(a), but is significantly altered due to the contact asymmetry, as shown in Fig. 6(b). Third and most important, although the photocurrent $I_{ph}$ is no longer a perfect sine function on the polarization angle, zero $I_{ph}$ still occurs at certain polarization angles and photon energies, as evidenced in Figs. 6(a) and 6(b). In other words, the nonideal spin battery still generates pure spin current even with the structural perturbations. Figures 6(c) and 6(d) present the calculated operational points of the nonideal spin battery in terms of the photon energy and polarization angle: these are to be compared with Fig. 4(c) for the ideal spin battery. We conclude that the spin battery works whether it is ideal or perturbed, albeit at some different photon energies and polarization angles. Importantly, the signature of pure spin-current generation is when the total photocurrent $I_{ph}$ vanishes, which provides the operational point of the device whether it is ideal or not.

It is interesting to investigate if the SOC effect will significantly alter the outcome of the spin battery. To this end, we carry out calculations for the same spin-battery system by including SOC in the first-principles analysis. The results show that the photocurrent is still a perfect $\sin(2\theta)$, as shown in Fig. 7, which qualitatively agrees well with the results where SOC is neglected.

In summary, we find that the 2D spin-battery device operating on the PGE can deliver a pure spin current without an accompanying charge current to the outside world, which is important for 2D flexible spintronics. The principle of the device is implemented in the 2D material phosphorene and first-principles calculations give numerical data that are in excellent qualitative agreement with the physics of the PGE. The PGE spin battery has excellent operational stability against structural disorder, photon energy and flux, and other material characteristics. The 2D spin battery is interesting as it is a device that generates pure spin currents, an energy source that harvests photons, as well as being a pure spin-current detector itself. Finally, given the recent experimental discovery of 2D ferromagnetism [54,55], the PGE spin battery may be entirely realized by layered materials.

## ACKNOWLEDGMENTS

Y.W. is grateful to Dr. Lei Liu, Dr. Yanxia Xing, and Dr. Chao-Cheng Kaun for useful discussions. This work was supported by the National Natural Science Foundation of China under Grants No. 11404273 and No. 11774217 (to Y.W.) and No. 51871156 (to Y.X.) and the University Grant Council (Contract No. AoE/P-04/08) of the Government of HKSAR (to Y.W., J.W., and H.G.).

[1] G. Fiori, F. Bonaccorso, G. Iannaccone, T. Palacios, D. Neumaier, A. Seabaugh, S. K. Banerjee, and L. Colombo, Electronics based on two-dimensional materials, Nat. Nanotechnol. **9**, 768 (2014).

[2] A. Nathan, A. Ahnood, M. T. Cole, S. Lee, Y. Suzuki, P. Hiralal, F. Bonaccorso, T. Hasan, L. Garcia-Gancedo, A. Dyadyusha, S. Haque, P. Andrew, S. Hofmann, J. Moultrie, D. Chu, A. J. Flewitt, A. C. Ferrari, M. J. Kelly, J. Robertson, G. A. J. Amaratunga, and W. I. Milne, Flexible electronics: The next ubiquitous platform, Proc. IEEE **100**, 1486 (2012).

[3] S. A. Wolf, D. D. Awschalom, R. A. Buhrman, J. M. Daughton, S. von Molnar, M. L. Roukes, A. Y. Chtchelkanova, and D. M. Treger, Spintronics: A spin-based electronics vision for the future, Science **294**, 1488 (2001).

[4] I. Zutic, J. Fabian, and S. D. Sarma, Spintronics: Fundamentals and applications, Rev. Mod. Phys. **76**, 323 (2004).

[5] M. Harder, Y. Gui, and C.-M. Hu, Electrical detection of magnetization dynamics via spin rectification effects, Phys. Rep. **661**, 1 (2016).

[6] V. I. Belinicher and B. I. Sturman, The photogalvanic effect in media lacking a center of symmetry, Sov. Phys. Usp. **23**, 199 (1980).

[7] S. Dhara, E. J. Mele, and R. Agarwal, Voltage-tunable circular photogalvanic effect in silicon nanowires, Science **349**, 726 (2015).

[8] P. Olbrich, S. A. Tarasenko, C. Reitmaier, J. Karch, D. Plohmann, Z. D. Kvon, and S. D. Ganichev, Observation of the orbital circular photogalvanic effect, Phys. Rev. B **79**, 121302 (2009).

[9] J. Karch, S. A. Tarasenko, E. L. Ivchenko, J. Kamann, P. Olbrich, M. Utz, Z. D. Kvon, and S. D. Ganichev, Photoexcitation of valley-orbit currents in (111)-oriented silicon metal-oxide-semiconductor field-effect transistors, Phys. Rev. B **83**, 121312 (2011).

[10] S. D. Ganichev, E. L. Ivchenko, V. V. Bel'kov, S. A. Tarasenko, M. Sollinger, D. Weiss, W. Wegscheider, and W. Prettl, Spin-galvanic effect, Nature **417**, 153 (2002).

[11] S. D. Ganichev, H. Ketterl, W. Prettl, E. L. Ivchenko, and L. E. Vorobjev, Circular photogalvanic effect induced by monopolar spin orientation in p-GaAs/AlGaAs multiple-quantum wells, Appl. Phys. Lett. **77**, 3146 (2000).

[12] S. D. Ganichev, E. L. Ivchenko, S. N. Danilov, J. Eroms, W. Wegscheider, D. Weiss, and W. Prettl, Conversion of Spin into Directed Electric Current in Quantum Wells, Phys. Rev. Lett. **86**, 4358 (2001).

[13] S. D. Ganichev and W. Prettl, Spin photocurrents in quantum wells, J. Phys.: Condens. Matter **15**, R935 (2003).

[14] C. Yin, H. Yuan, X. Wang, S. Liu, S. Zhang, N. Tang, F. Xu, Z. Chen, H. Shimotani, Y. Iwasa, Y. Chen, W. Ge, and B. Shen, Tunable surface electron spin splitting with electric double-layer transistors based on InN, Nano Lett. **13**, 2024 (2013).

[15] H. Yuan, X. Wang, B. Lian, H. Zhang, X. Fang, B. Shen, G. Xu, Y. Xu, S.-C. Zhang, H. Y. Hwang, and Y. Cui, Generation and electric control of spin-valley-coupled circular photogalvanic current in $WSe_2$, Nat. Nanotechnol. **9**, 851 (2014).

[16] M. Eginligil, B. Cao, Z. Wang, X. Shen, C. Cong, J. Shang, C. Soci, and T. Yu, Dichroic spin-valley photocurrent in monolayer molybdenum disulphide, Nat. Commun. **6**, 7636 (2015).

[17] C. Kastl, C. Karnetzky, H. Karl, and A. W. Holleitner, Ultrafast helicity control of surface currents in topological insulators with near-unity fidelity, Nat. Commun. **6**, 6617 (2015).

[18] K. N. Okada, N. Ogawa, R. Yoshimi, A. Tsukazaki, K. S. Takahashi, M. Kawasaki, and Y. Tokura, Enhanced photogalvanic current in topological insulators via Fermi energy tuning, Phys. Rev. B **93**, 081403 (2016).

[19] J. W. McIver, D. Hsieh, H. Steinberg, P. Jarillo-Herrero, and N. Gedik, Control over topological insulator photocurrents with light polarization, Nat. Nanotechnol. **7**, 96 (2012).

[20] G. E. W. Bauer, E. Saitoh, and B. J. van Wees, Spin caloritronics, Nat. Mater. **11**, 391 (2012).

[21] J. Tian, S. Hong, I. Miotkowski, S. Datta, and Y. P. Chen, Observation of current-induced, long-lived persistent spin polarization in a topological insulator: A rechargeable spin battery, Sci. Adv. **3**, e1602531 (2017).

[22] J. E. Hirsch, Spin Hall Effect, Phys. Rev. Lett. **83**, 1834 (1999).

[23] D. Ellsworth, L. Lu, J. Lan, H. Chang, P. Li, Z. Wang, J. Hu, B. Johnson, Y. Bian, J. Xiao, R. Wu, and M. Wu, Photo-spin-voltaic effect, Nat. Phys. **12**, 861 (2016).

[24] Y. Kajiwara, K. Harii, S. Takahashi, J. Ohe, K. Uchida, M. Mizuguchi, H. Umezawa, H. Kawai, K. Ando, K. Takanashi, S. Maekawa, and E. Saitoh, Transmission of electrical signals by spin-wave interconversion in a magnetic insulator, Nature **464**, 262 (2010).

[25] S. W. Jiang, S. Liu, P. Wang, Z. Z. Luan, X. D. Tao, H. F. Ding, and D. Wu, Exchange-Dominated Pure Spin Current Transport in $Alq_3$ Molecules, Phys. Rev. Lett. **115**, 086601 (2015).

[26] J. B. S. Mendes, O. Alves Santos, L. M. Meireles, R. G. Lacerda, L. H. Vilela-Leão, F. L. A. Machado, R. L. Rodríguez-Suárez, A. Azevedo, and S. M. Rezende, Spin-Current to Charge-Current Conversion and Magnetoresistance in a Hybrid Structure of Graphene and Yttrium Iron Garnet, Phys. Rev. Lett. **115**, 226601 (2015).

[27] K. Uchida, S. Takahashi, K. Harii, J. Ieda, W. Koshibae, K. Ando, S. Maekawa, and E. Saitoh, Observation of the spin Seebeck effect, Nature **455**, 778 (2008).

[28] D. Meier, T. Kuschel, L. Shen, A. Gupta, T. Kikkawa, K. Uchida, E. Saitoh, J.-M. Schmalhorst, and G. Reiss, Thermally driven spin and charge currents in thin $NiFe_2O_4$/Pt films, Phys. Rev. B **87**, 054421 (2013).

[29] P. Li, D. Ellsworth, H. Chang, P. Janantha, D. Richardson, F. Shah, P. Phillips, T. Vijayasarathy, and M. Wu, Generation of pure spin currents via spin Seebeck effect in self-biased hexagonal ferrite thin films, Appl. Phys. Lett. **105**, 242412 (2014).

[30] W. Lin, K. Chen, S. Zhang, and C. L. Chien, Enhancement of Thermally Injected Spin Current Through an Antiferromagnetic Insulator, Phys. Rev. Lett. **116**, 186601 (2016).

[31] J. F. Sierra, I. Neumann, J. Cuppens, B. Raes, M. V. Costache, and S. O. Valenzuela, Thermoelectric spin voltage in graphene, Nat. Nanotechnol. **13**, 107 (2018).

[32] L. Berger, Generation of dc voltages by a magnetic multilayer undergoing ferromagnetic resonance, Phys. Rev. B **59**, 11465 (1999).

[33] G. Schmidt, D. Ferrand, L. W. Molenkamp, A. T. Filip, and B. J. van Wees, Fundamental obstacle for electrical spin injection from a ferromagnetic metal into a diffusive semiconductor, Phys. Rev. B **62**, R4790 (2000).

[34] E. I. Rashba, Theory of electrical spin injection: Tunnel contacts as a solution of the conductivity mismatch problem, Phys. Rev. B **62**, R16267 (2000).

[35] A. Brataas, Y. Tserkovnyak, G. E. W. Bauer, and B. I. Halperin, Spin battery operated by ferromagnetic resonance, Phys. Rev. B **66**, 060404(R) (2002).

[36] L. Li, Y. Yu, G. J. Ye, Q. Ge, X. Ou, H. Wu, D. Feng, X. H. Chen, and Y. Zhang, Black phosphorus field-effect transistors, Nat. Nanotechnol. **9**, 372 (2014).

[37] J. Qiao, X. Kong, Z.-X. Hu, F. Yang, and W. Ji, High-mobility transport anisotropy and linear dichroism in few-layer black phosphorus, Nat. Commun. **5**, 4475 (2014).

[38] V. Tran, R. Soklaski, Y. Liang, and L. Yang, Layer-controlled band gap and anisotropic excitons in few-layer black phosphorus, Phys. Rev. B **89**, 235319 (2014).

[39] M. Buscema, D. J. Groenendijk, G. A. Steele, H. S. J. van der Zant, and A. Castellanos-Gomez, Photovoltaic effect in few-layer black phosphorus PN junctions defined by local electrostatic gating, Nat. Commun. **5**, 4651 (2014).

[40] M. Buscema, D. J. Groenendijk, S. I. Blanter, G. A. Steele, H. S. J. van der Zant, and A. Castellanos-Gomez, Fast and broadband photoresponse of few-layer black phosphorus field-effect transistors, Nano Lett. **14**, 3347 (2014).

[41] T. Hong, B. Chamlagain, W. Lin, H.-J. Chuang, M. Pan, Z. Zhou, and Y.-Q. Xu, Polarized photocurrent response in black phosphorus field-effect transistors, Nanoscale **6**, 8978 (2014).

[42] Q. Guo, A. Pospischil, M. Bhuiyan, H. Jiang, H. Tian, D. Farmer, B. Deng, C. Li, S.-J. Han, H. Wang, Q. Xia, T.-P. Ma, T. Mueller, and F. Xia, Black phosphorus mid-infrared photodetectors with high gain, Nano Lett. **16**, 4648 (2016).

[43] M. V. Kamalakar, B. N. Madhushankar, A. Dankert, and S. P. Dash, Low Schottky barrier black phosphorus field-effect devices with ferromagnetic tunnel contacts, Small **11**, 2209 (2015).

[44] M. Huang, M. Wang, C. Chen, Z. Ma, X. Li, J. Han, and Y. Wu, Broadband black-phosphorus photodetectors with high responsivity, Adv. Mater. **28**, 3481 (2016).

[45] G. Kresse and J. Furthmüller, Efficient iterative schemes for *ab initio* total-energy calculations using a plane-wave basis set, Phys. Rev. B **54**, 11169 (1996).

[46] Y. Xie, L. Zhang, Y. Zhu, L. Liu, and H. Guo, Photogalvanic effect in monolayer black phosphorus, Nanotechnology **26**, 455202 (2015).

[47] J. Taylor, H. Guo, and J. Wang, *Ab initio* modeling of quantum transport properties of molecular electronic devices, Phys. Rev. B **63**, 245407 (2001).

[48] J. Wu, G. K. W. Koon, D. Xiang, C. Han, C. T. Toh, E. S. Kulkarni, I. Verzhbitskiy, A. Carvalho, A. S. Rodin, S. P. Koenig, G. Eda, W. Chen, A. H. C. Neto, and B. Ozyilmaz, Colossal ultraviolet photoresponsivity of few-layer black phosphorus, ACS Nano **9**, 8070 (2015).

[49] C. Kamal and M. Ezawa, Arsenene: Two-dimensional buckled and puckered honeycomb arsenic systems, Phys. Rev. B **91**, 085423 (2015).

[50] B. Liu, M. Kopf, A. N. Abbas, X. Wang, Q. Guo, Y. Jia, F. Xia, R. Weihrich, F. Bachhuber, F. Pielnhofer, H. Wang, R. Dhall, S. B. Cronin, M. Ge, X. Fang, T. Nilges, and C. Zhou, Black arsenic phosphorus: Layered anisotropic infrared semiconductors with highly tunable compositions and properties, Adv. Mater. **27**, 4423 (2015).

[51] Z. Zhu, J. Guan, and D. Tománek, Structural transition in layered $As_{1-x}P_x$ compounds: A computational study, Nano Lett. **15**, 6042 (2015).

[52] S. O. Valenzuela and M. Tinkham, Direct electronic measurement of the spin Hall effect, Nature **442**, 176 (2006).

[53] D. Sun, J. v. Schootech, M. Kavand, H. Malissa, C. Zhang, M. Groesbeck, C. Boehme, and Z. V. Vardeny, Inverse spin Hall effect from pulsed spin current in organic semiconductors with tunable spin-orbit coupling, Nat. Mater. **15**, 863 (2016).

[54] C. Gong, L. Li, Z. Li, H. Ji, A. Stern, Y. Xia, T. Cao, W. Bao, C. Wang, Y. Wang, Z. Q. Qiu, R. J. Cava, S. G. Louie, J. Xia, and X. Zhang, Discovery of intrinsic ferromagnetism in two-dimensional van der Waals crystals, Nature **546**, 265 (2017).

[55] B. Huang, G. Clark, E. Navarro-Moratalla, D. R. Klein, R. Cheng, K. L. Seyler, D. Zhong, E. Schmidgall, M. A. McGuire, D. H. Cobden, W. Yao, D. Xiao, P. Jarillo-Herrero, and X. Xu, Layer-dependent ferromagnetism in a van der Waals crystal down to the monolayer limit, Nature **546**, 270 (2017).